Research on Mechanical Characteristics and Load-bearing Behavior of Nodes of Steel Fiber Concrete Arch Bridges

Liu Kailiang* and Wang Sen

Zhengzhou Railway Vocational & Technical College, Zhengzhou Henan 450000, China
E-mail: liukailiang@zzrvtc.edu.cn
**Corresponding Author*

Received 22 May 2023; Accepted 26 June 2023;
Publication 30 September 2023

Abstract

Steel fiber reinforced concrete (SFRC) is a new type of composite material formed by dispersing discontinuous short steel fibers in a uniform and random direction throughout the concrete, which has excellent properties of tensile, shear and high toughness, can effectively improve the load-bearing capacity of arch bridges. In this paper, the mechanics of SFRP in the nodal structure of an arch bridge is initially explored by means of indoor model tests and numerical simulation studies. The results show that the maximum principal tensile stress occurs at the intersection of arch rib, arch foot and tie beam, and the maximum principal compressive stress occurs at the connection between arch rib and arch seat, which should be considered in the design. In this paper, we hope to understand the characteristics of the force and bearing capacity of this type of structure to provide a reference for similar projects.

Keywords: Steel fiber reinforced concrete, arch bridge structure, finite element method, carrying capacity.

European Journal of Computational Mechanics, Vol. 32_3, 211–234.
doi: 10.13052/ejcm2642-2085.3231

1 Introduction

In recent years, the application of steel fiber reinforced concrete (SFRC) in industrial and civil buildings, road and bridge construction, and hydraulic engineering has achieved good economic results. However, it is rarely used in underground projects and is still being tested [1]. In addition to the complexity of underground structures, spraying equipment, spraying technology, and stress conditions of steel fiber products, it is also related to the imperfection of the structural design calculation theory of concrete and the lack of certain engineering experience [2]. SFRP is essentially steel fibers added to concrete, and it is more complex from material combination to stress conditions. According to the available test results, the basic performance of SFRC depends mainly on the nature of the matrix, while steel fibers can only improve its crack resistance and toughness [3]. On this basis, the mechanism of steel fiber-reinforced concrete has been explored more at home and abroad. From the structural level to fracture mechanics, there are many basic ideas so far, among which the use of composite mechanics (hybrid law) and the fracture mechanics-based fiber spacing theory are dominant [4]. The current research has gone further to the microstructural level and analyzed the strengthening mechanism at the tissue level. However, there is still a lack of a mature relationship between the intrinsic structure of SFRP and the corresponding systematic theoretical studies [5]. The research on the influence of steel fiber reinforced concrete on the mechanical properties and damage modes of the entire lining in tunnel lining is still relatively weak, especially in China. The application research of steel fiber reinforced concrete in underground engineering started relatively late in China, and has mainly relied on examples from steel tunnel projects overseas, as well as on its application in building construction, bridges, and other fields domestically [6], as well as the proposed fracture mechanics design method for SFRP tunnel linings Taken together, it is generally considered that the engineering effect and economic benefit is better than that of steel reinforced concrete, but it is reasonable to optimize the design of tunnel support suitable for Chinese engineering geological conditions, even though the design is generally conservative, the method still has great practical value [7–9]. Therefore, the study of the mechanical properties and bearing capacity of SFRC lining will play an important role in the selection of various parameters and the optimal design of the whole lining structure [10, 11]. This paper will analyze the current application examples of SFRP in arch bridge projects from different perspectives by studying the structural force and deformation data simulations

of SFRP and the description of construction key process parameters in practical engineering applications, and the research data and conclusions will be of good significance for future similar engineering applications and studies [12, 13].

In 1910, H. Porter of the United States presented the first research report on short steel fiber reinforced concrete. In 1963, J.P. Romualdi and G.B. Batson published a series of papers on the crack resistance mechanism of steel fibers, proposing the famous steel fiber reinforced concrete reinforcement theory: the "Fiber Spacing Theory", which has been widely applied in practice. Since then, the United States, Britain, Japan, and other countries have developed advanced manufacturing techniques such as the milling method and melt extraction method, thus making it well developed in industry research and practical application [14, 15].

SFRP consists of the following components: cement, distribution direction dispersion of short steel fibers. Steel fibers are effective in preventing cracking, improving its resistance to cracking, increasing the ductility and elasticity of the material, and thus maintaining good material properties at very low temperatures [16]. Hebpocab added metal to ordinary concrete in 1906. In Europe and the United States and other countries in 1941 a large number of tests on short steel concrete, found that short steel fiber in the prevention of cracks, improve the strength of a better effect. In addition, a lot of research and experiments were conducted to improve the production process, so there was no problem in the production of this material. In 1962, Romualdi and Batson achieved significant results in SFRP and analyzed its cracking mechanism, and concluded that the strength of cracks was closely related to the spacing between short steel fibers [17]. The results of this study truly introduced SFRP for construction projects. To date, through continued development, the material has gained widespread use in practice [18]. Although the incorporation of fibers was found to be effective in improving its mechanical properties and toughness, the theoretical analysis in this area is not yet complete [19]. In the current academic community, the study of composite theory and fiber spacing theory is still generally accepted in the community [20]. The former is the reinforcing effect of researchers adding brittle fracture fibers and additives to the matrix. It has been shown that the addition of fibers does not have much effect on the properties of the matrix and that the mixing law can be used directly in the calculation of material properties. The fiber spacing theory, also known as blockage theory, was proposed by Romualdi and Batson in the late 20th century [21]. The theory suggests that there is only one element that can change the properties of a

material, namely fiber spacing [22]. Both of these methods do not adequately reflect the strengthening effect of fibers, so when their theories were established, they were not applied to the problem of preventing material cracking. The biggest problem with the latter is that when this aspect of the analysis was conducted, the study was examined only one-sidedly and was not considered as a whole, exploring its function from only one aspect and pointing out that fiber spacing is the only determinant of performance.

As an innovative engineering material and structural form, steel fiber reinforced concrete arch bridge has many advantages and broad application prospects. The steel fiber reinforced concrete arch bridge combines the advantages of steel fiber and concrete to provide a high-performance, high-strength and durable building material for bridge engineering. Steel fibers can effectively resist and limit the expansion of cracks, improve the earthquake resistance and wind resistance of the structure, thereby improving the overall safety of the arch bridge, enhancing the tensile strength and ductility of concrete, and improving the overall stiffness and bearing capacity of the arch bridge structure ability. This enables steel fiber reinforced concrete arch bridges to carry greater loads and span longer spans. At the same time, steel fibers can prevent cracking and corrosion of concrete and delay the aging process of the structure. The use of this material reduces maintenance and restoration costs and extends the life of the arch bridge.

The application prospect of steel fiber reinforced concrete arch bridge is very broad. They can be used in different types of arch bridges including road bridges, railway bridges and pedestrian bridges etc. In addition, steel fiber reinforced concrete arch bridges can also be used in complex geological conditions and harsh environments, such as ocean bridges and bridges in alpine regions. With the continuous improvement of the requirements for the safety and durability of bridge structures, steel fiber reinforced concrete arch bridges will become an important choice for future bridge engineering.

All in all, steel fiber reinforced concrete arch bridges have broad application prospects due to their advantages in crack resistance, bearing capacity, durability, construction efficiency, and sustainability. This material and structural form will play an important role in the field of bridge engineering, providing people with safer, more reliable and more economical bridge solutions.

The essence of SFRP is the addition of steel fibers in concrete, a multiphase composite material to become a more complex composite material from the combination of materials to the force situation [23]. From existing tests, it can be found that the inherent properties of steel fiber reinforced

concrete are mostly determined by the properties of the matrix concrete, and the addition of steel fibers only enhances the crack resistance and toughness of the concrete [24]. A large number of studies have been conducted at home and abroad on the strengthening mechanism of SFRP, and so far its basic ideas from the structural level to fracture mechanics have a variety of, mainly the use of composite mechanical theory mixed rate law and fracture mechanics based on the fiber spacing theory. The current research has further deepened to the fine structure level to analyze the strengthening mechanism from the organization level. However, there is still a lack of mature SFRP principal structure relationship and the corresponding systematic theoretical research, its application in the arch bridge on the entire bridge mechanical behavior and the impact of damage form is still very weak research [25].

2 Basic Characteristics of SFRP Arch Bridge

SFRP is a new type of composite material, which has better tensile, crack resistance, and durability properties, thus it is widely used in bridges, tunnels, subways, and other engineering construction fields. As an important type of bridge, SFRP arch bridge has the advantages of structural stability, lightweight, and easy construction, which has become an important part of bridge construction in the world today. In this paper, we will start with the basic characteristics of SFRP arch bridges and systematically discuss their structural characteristics, mechanical properties, and design points, to provide some reference for the design and practical application of bridge engineering.

2.1 Structural Characteristics of SFRP Arch Bridge

SFRP arch bridge is a typical curved structure, which mainly consists of arch ribs and arch foot piers, in the middle of which can be set bridge deck, railings, and other components. The cross-section of the arch bridge is usually an equilateral triangle, round, oval, and other shapes, the arch belly is curved, and the arch foot pier is mostly rectangular or polygonal. Figure 1 is a typical SFRP arch bridge diagram.

The main load-bearing structure of an arch bridge is the arch rib, whose form and quantity directly affect the mechanical characteristics and engineering cost of the arch bridge. In actual engineering, the form of arch rib is usually in the form of arc or oval, the number is generally 1–3, in most cases two, located on both sides of the bridge pier. The axis of the arch ribs

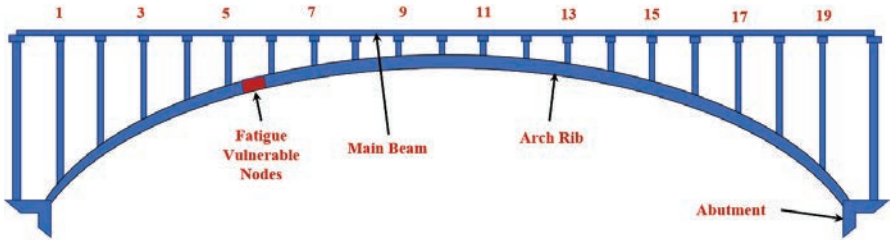

Figure 1 Schematic diagram of SFRP arch bridge.

can be perpendicular to the bridge deck or have a certain inclination with the bridge deck, different axis designs can achieve different functional and aesthetic effects of the arch bridge.

The arch foot pier is the bearing of the arch bridge, which plays the role of load bearing, support, and stability. In the SFRP arch bridge, the arch foot pier usually adopts reinforced concrete or SFRP structure, its structure form can be single pier type or continuous pier type. Single pier type arch foot pier is located at the ends of the arch ribs, mostly rectangular or polygonal, easy for construction and maintenance, but for large span arch bridge, single pier type structure will increase the height and volume of the arch foot pier, affecting the aesthetic and navigational conditions. Therefore, continuous pier structure is widely used in large-span arch bridges, which can effectively reduce the height and volume of arch foot piers and improve the economy and aesthetics of arch bridges.

The bearing of the arch bridge is an important connecting part of the bridge structure, whose function is to transfer the bridge load and deformation, and at the same time to ensure the operational safety of the bridge. The support form of SFRP arch bridge includes rubber bearings, spherical bearings, and sliding bearings, among which rubber bearing is the most commonly used one. Rubber bearing has better vibration damping and sound insulation effect, which can reduce the vibration and noise of the bridge structure, and also has better durability and easy maintenance.

2.2 Mechanical Properties of SFRP Arch Bridges

The mechanical characteristics of SFRP arch bridge refer to the force, deformation, and damage characteristics of the arch bridge under the action of load [26]. The mechanical properties of SFRP arch bridge are influenced by the form of arch rib, arch foot pier structure, support form, and other factors, which have certain characteristics and regularity.

As the main load-bearing structure of the arch bridge, the force characteristics of arch ribs directly affect the load-bearing capacity and stability of the arch bridge. The arch rib of a SFRP arch bridge is mainly subjected to bending and shear, and there are also certain axial and transverse forces. Under the load, the shear force and bending moment of the arch rib are large, so the cross-sectional shape and size of the arch rib need to be reasonably selected to meet its strength and stiffness requirements.

The arch foot pier as a bearing, its bearing capacity is mainly affected by the foundation and load. The arch foot pier of SFRP arch bridge has a certain moment and shear bearing capacity and needs to meet its strength and stability requirements under load. At the same time, the volume and height of the arch foot pier have a great influence on the economy and aesthetics of the arch bridge, so it is necessary to optimize the arch foot pier structure to improve its bearing capacity and reduce the volume.

As an important connecting part of the bridge structure, the bearing capacity and deformation of the bearings have an important influence on the operational safety and comfort of the bridge. The bearings of SFRP arch bridges have better vibration damping and sound insulation effects but also need to meet certain load-bearing capacity and deformation requirements. Therefore, it is necessary to reasonably select the bearing form and material and also carry out bearing design and construction.

The deformation of SFRP arch bridges is mainly in the form of arch top subsidence and arch waist torsion, and there are also certain transverse displacement and axial deformation. Under the action of load, the arch top sinking and arch waist twisting are more obvious, so it is necessary to reduce the deformation by reasonable design of the arch rib section and support form.

During the design and construction of arch bridges, the deformation of arch bridges needs to be controlled and compensated. Among them, the main ways to control the deformation include reasonable selection of arch rib section, arch foot pier and bearing reinforcement, etc. Measures such as deformation monitoring and evaluation are also required. The deformation that has occurred, it can be solved by adjusting the support and taking compensation measures. Different forms of damage may occur in SFRP arch bridges under load, which mainly include bending damage of arch ribs, collapse damage of arch foot piers, and failure damage of bearings. In the design and construction of arch bridges, reasonable structural design and construction quality control are needed to ensure the safe operation of arch bridges, and damage simulation and evaluation are also needed to predict the damage forms and damage loads of arch bridges.

SFRP arch bridges have better mechanical and economic properties and are widely used in bridge engineering. The addition of SFRP can improve the load-carrying and deformation performance of arch bridges, reduce structural volume, and improve the economy of bridges. In the design and construction of SFRP arch bridges, the mechanical properties, deformation performance, and damage performance of the structure need to be considered. By means of reasonable structural design and quality control of construction, the safe operation of the arch bridge can be ensured.

3 Stress Analysis of SFRP Beam Section

In steel fiber reinforced concrete structures, vertical cracks may occur in concrete members due to external loads. The presence of these cracks can lead to the appearance of normal tensile stress in the concrete. However, under the first stage of loading, vertical cracks have already appeared, and the normal tensile stress in the concrete has been dispersed into the cracks, which does not have a significant impact on the overall performance of the structure. Therefore, we can ignore the normal tensile stress in concrete.

Under the first stage load, the steel fiber will be subjected to tensile stress and bear part of the tensile load. Therefore, we need to consider the tensile effect of steel fibers to accurately evaluate the tensile performance of the structure.

In order to carry out mechanical analysis and calculation, we usually simplify complex phenomena. In this case, we simplify the tensile stress provided by the steel fibers into a rectangular distribution. This simplification can simplify calculations and provide sufficiently accurate results.

It is assumed that vertical cracks have appeared in the beam under the first stage of loading, thus the positive tensile stress in the concrete can be ignored [27], but the tensile effect of steel fibers needs to be considered and the tensile stress provided by the steel fibers is simplified into a rectangular distribution diagram, as shown in Figure 2, and the equilibrium relationship of the internal forces by the diagram, there are:

$$\sum F_x = 0,\ T_{sl} + dT_{sl} + (\sigma_{ft} + d\sigma_{ft})bh_y = T_{sl} + d\sigma_{ft}bh_y + \tau_l bdx,$$

$$\tau_l = \frac{l}{b}\frac{dT_{sl}}{dx} + h_y\frac{d\sigma_{ft}}{dx} \tag{1}$$

$$\sum M_C = 0,\ M_l = T_{sl}\eta_1 h_{0l} + T_{nl}\eta_2 h_{0l} \tag{2}$$

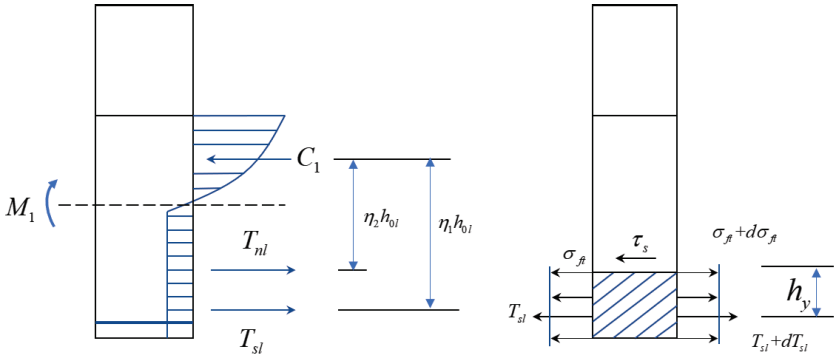

Figure 2 Stress distribution of SFRP beam section.

In Equations (1), (2), $\sum F$ is x The equilibrium force in the direction, $\sum M$ is the equilibrium bending moment; η_1 and η_2 are the internal force arm factor; τ_1 is the shear stress in the precast beam at h_y, σ_{ft} is the equivalent tensile stress in the precast beam steel fibers, b is the width of the beam, h_{01} is the beam height.

Differentiating both sides of Equation (2), there are tensions:

$$V_1 = \frac{dM_1}{dx} = \eta_1 h_{01} \frac{dT_{sl}}{dx} + \eta_2 h_{01} \frac{dT_{nl}}{dx} \tag{3}$$

From the stress-strain relationship, it is obtained that:

$$T_{sl} = E_s A_s \varepsilon_{sl} \tag{4}$$

$$T_{nl} = \sigma_{ft} A_{ft} + E_f A_f \varepsilon_{nl} \tag{5}$$

where, A_s and A_f are the total transverse area of the reinforcement and steel fiber in tension, E_s and E_f are the moduli of elasticity of the reinforcement and steel fiber, and ε_{sl} and ε_{nl} are the strain of the reinforcement and beam, respectively.

Differentiating the two sides of Equation (5) yields:

$$\frac{dT_{nl}}{dx} = A_f \frac{d\sigma_{sl}}{dx} \tag{6}$$

from Figure 2(c), we can see that

$$\varepsilon_{sl} = 2\varepsilon_{nl} \tag{7}$$

substituting Equation (7) into Equations (4) and (5), we get

$$T_{nl} = \frac{A_f}{2A_s} T_{sl} \tag{8}$$

differentiating both sides of Equation (8) yields

$$\frac{dT_{nl}}{dx} = \frac{A_f}{2A_s} \frac{dT_{sl}}{dx} \tag{9}$$

substituting Equation (9) into Equation (3), we get

$$\frac{dT_{sl}}{dx} = \frac{1}{\left|\eta_1 + \eta_2 \frac{A_f}{2A_s}\right| h_{01}} V_l \tag{10}$$

substituting Equation (9) into Equation (6), we get

$$\frac{d\sigma_{ft}}{dx} = \frac{A_f}{2A_s} \frac{dT_{sl}}{dx} \tag{11}$$

substituting Equation (11) and Equation (10) into Equation (1), we get

$$\tau_l = \left|\frac{1}{b} + \frac{h_y}{2A_s}\right| \frac{dT_{sl}}{dx} = \frac{\frac{1}{b} + \frac{h_y}{2A_s}}{\left|\eta_1 + \eta_2 \frac{A_f}{2A_s}\right| h_{01}} V_l \tag{12}$$

in the formula, τ_l is the shear stress of the whole beam at h_y, *N/mm*^{2}, h_{01} is the height of the whole beam, *mm*.

4 Loading Test in Laboratory

4.1 Specimen Design

A 130 m span hollow box arch bridge in southwest China was selected as the supporting project, and the height of the web row frame columns ranged from 1.680 to 10.584 m, of which the height of the No. 6 row frame column was 2.894 m, with moderate length-to-thin ratio, and its size was suitable and met the indoor test conditions, so No. 6 row frame column was selected as the research prototype to produce the test specimen.

One of the reasons for choosing bend column No. 6 is its medium slenderness ratio. The slenderness ratio refers to the ratio of the length of the structure in the longitudinal direction to the cross-sectional size. The test

specimen with medium slenderness ratio is more in line with the engineering scale of the actual arch bridge, and can better simulate the mechanical behavior in the actual engineering situation. The mechanical properties of actual arch bridge structures with similar slenderness ratios can be more accurately evaluated and predicted through experimental studies on curved columns with moderate slenderness ratios.

4.2 Loading Solutions

The proposed static test (also known as low circumferential reciprocal load test) is a low circumferential reciprocal loading of the test body through load control or deformation control so that the test body is from the elastic stage until the destruction of the whole process test. Figure 3 is a schematic diagram of the loading device. The test can approximate the reciprocal vibration process of the structure under the action of the earthquake and is a common method to study the force and deformation performance of the structure. The test vertical load is loaded to a predetermined axial force of 167.91 kN by jack (simulating the top load of a real bridge column) and maintained constant; the horizontal load is controlled by displacement, before yielding, the loading amplitude is 1 mm, after reaching the yielding displacement, the loading amplitude is 2 mm, and each loading cycle is repeated three times; when the peak of the horizontal load in the cycle falls to the specimen When the peak of the horizontal load in the cycle drops to 83% of the ultimate load, the loading is stopped.

Test program design: (1) synchronous loading of axial force and annular confining pressure so that the axial and annular stresses are equal in the same time; (2) keep the confining pressure constant, and realize the axial force Add and uninstall. Among them, there are 4 to 5 loading and unloading cycles before the peak stress, and 10 to 15 loading and unloading cycles after the peak stress; (3) Unloading the confining pressure and unloading the axial force.

4.3 Analysis of Test Results

To reveal the energy evolution and distribution law of SFRP material from initial deformation to damage under different circumferential pressure cycles, a series of tests with different circumferential pressure conditions under constant strain rate were carried out, and the stress-strain curves of the specimens are shown in Figures 4 to 6.

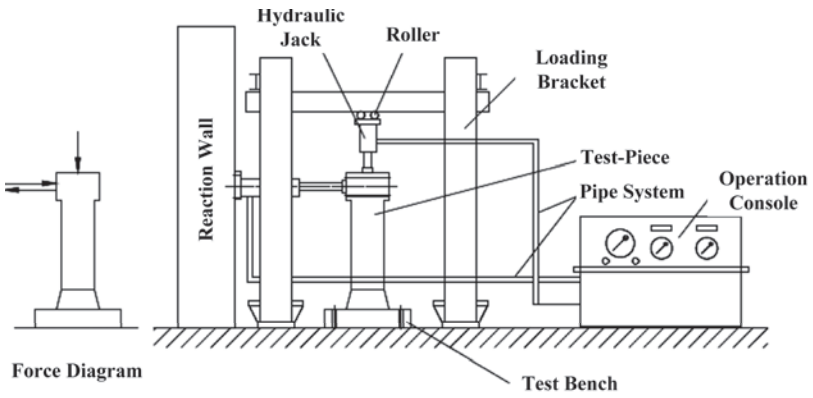

Figure 3 Loading device.

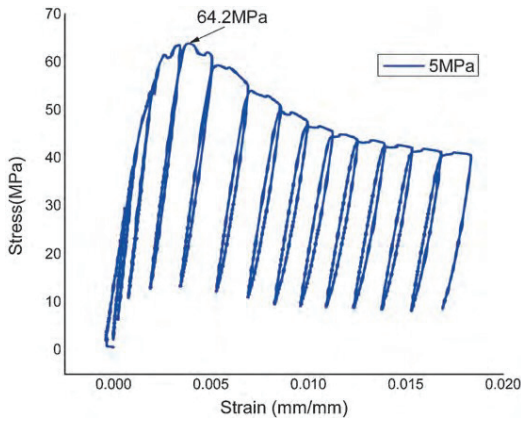

Figure 4 Stress-strain curve/peripheral pressure 5 MPa.

The following conclusions can be drawn from the analysis of the test results;

(1) The stress-strain curve of SFRP material under the action of triaxial cyclic loading and unloading has a hysteresis loop effect, because SFRP is a non-homogeneous ideal elastic material, taking into account the micro-cracks and micro-porosity of the material itself when the specimen is loaded to a certain stress value and then unloaded, the stress path of unloading does not coincide with the loaded stress path, and then a closed loop of the stress-strain curve is formed. The hysteresis loop is a closed loop of the stress-strain curve. The area of the

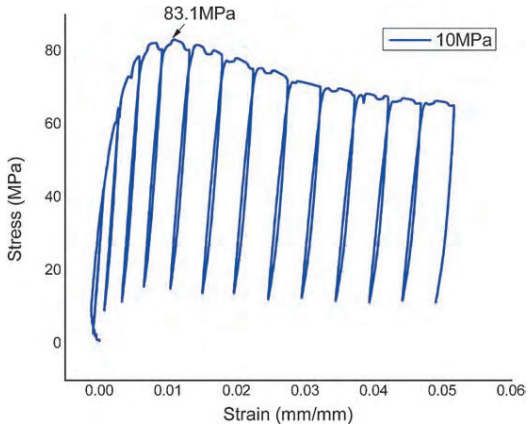

Figure 5 Stress-strain curve/peripheral pressure 10 MPa.

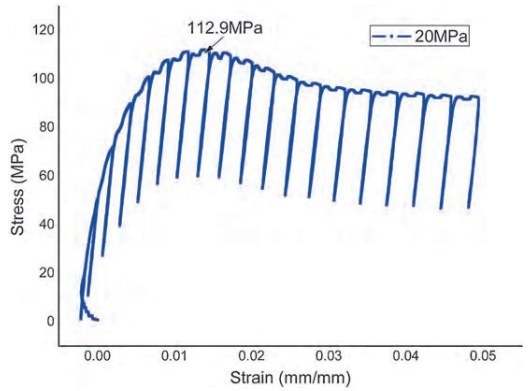

Figure 6 Stress-strain curve/peripheral pressure 20 MPa.

hysteresis loop characterizes the energy consumed in the whole process of crack appearance, expansion, closure, penetration, and destruction of the specimen from the time of loading.

(2) The maximum area of the hysteresis loop usually appears near the peak stress of the material, that is, the specimen at this time there is a large macro crack or the dissipation energy required for damage is larger. As the surrounding pressure increases, the stress point corresponding to the largest area of the hysteresis loop is then delayed, because the surrounding pressure effectively inhibits the development of cracks, while enhancing the plastic mechanical properties of the material.

(3) The stress-strain curve after the peak stress becomes flat and the plastic deformation characteristics of the material become obvious as the enclosing pressure increases. With the increase of the enclosing pressure, the strain after the peak stress becomes larger, but the stress changes little, reflecting the weak ductile damage characteristics of the material; and the peak stress of the material increases obviously, indicating that the enclosing pressure can effectively improve the strength and inhibit the deformation of the material.
(4) The stress-strain curve of the steel fiber reinforced concrete material under the action of triaxial cyclic loading and unloading appears a closed loop area, that is, the hysteresis loop effect. The largest area of the hysteresis loop usually appears near the peak stress of the material, and as the confining pressure increases, the stress point corresponding to the largest hysteresis loop appears later. With the continuous increase of the confining pressure, the strain increases significantly after the peak strain corresponding to the peak stress, but the stress changes little. The stress-strain curve of the material tends to be flat, reflecting the characteristics of plastic deformation, and the peak stress of the material increases obviously.

5 Finite Element Simulation Analysis

5.1 Finite Element Model

The main bridge is a calculated span L = 115 m under-bearing steel pipe concrete tied arch bridge, the arch rib is made of dumbbell type steel pipe concrete structure, the boom is made of steel stranded whole bundle extruded finished cable, the tied beam, end crossbeam, and middle crossbeam are made of prestressed concrete structure, the wind brace is made of empty steel pipe structure, the vehicle load class is highway-I, the steel is made of Q345D steel. After the full bridge model was established by finite element software, the internal force at the location of the arch ribs of the arch foot was extracted and the finite element model was established [28].

According to the design drawings, the finite element model includes the 2.0 m long dumbbell arch rib protruding from the foot of the arch, the solid part of the foot of the arch, half of the length of 5.95 m of the end crossbeam, and the 6 m section of the arch seat tie beam from the center line of the support. Through the calculation of the full bridge rod system model, the internal force of the arch rib section was obtained according to the most

unfavorable load combination of arch footing, and the section loading was selected in the arch rib and longitudinal beam respectively.

Among them, a support reaction force of 24260 kN is applied at the foot of the arch, an axial force of 29897 kN, a shear force of 58 kN and a bending moment of 3865 kN-m are applied to the arch rib, and an axial force of 21685 kN, a shear force of 132 kN and a bending moment of 2037 kN-m are applied at the truncated interface of the longitudinal beam.

The node at the location of the arch foot of the arch rib of the steel pipe concrete arch bridge is a key part of the overall structural stress range of the arch bridge, the steel pipe concrete bond structure through the concrete of the arch seat, in its contact position is extremely critical, followed by the existence of the arch rib, longitudinal beam and many other components in the bridge, under the action of large negative bending moment, the force at this location is more critical. Therefore, according to the specific size of the structure, a large general finite element program was used to establish the calculation model. To avoid the influence of the boundary conditions of the arch ribs on the study area, the interception length of the main arch ribs was more than twice the diameter.

At the bollard prestressing anchorage and end crossbeam prestressing anchorage, the surface load is applied to the anchor pad according to the actual prestressing effect, and the nodes are established at the center of mass position on the loading surface of the arch ribs and longitudinal beams, forming rigid arm units with other points on the loading surface, and finally, the nodal loads such as axial force, shear force and bending moment are applied on the loading surface. At the same time, the solid reaction force is applied at the bottom of the arch seat in the Y direction, and solid restraint is applied at the end of the end crossbeam.

5.2 Stress Analysis

The maximum principal compressive stress in the model is shown in Figure 7.

It can be seen from the figure that the maximum principal compressive stress can reach 30 MPa at the very individual points where the dumbbell-shaped arch ribs are embedded in the arch seat position, which is because the connection between the arch ribs and the arch seat, the load on the arch ribs is transferred to the connection, causing the local stress to increase at this place, followed by the turning point where the arch seat is connected with the arch ribs, the maximum principal compressive stress is 13 MPa, which is because the load transferred down from the arch ribs The maximum tensile

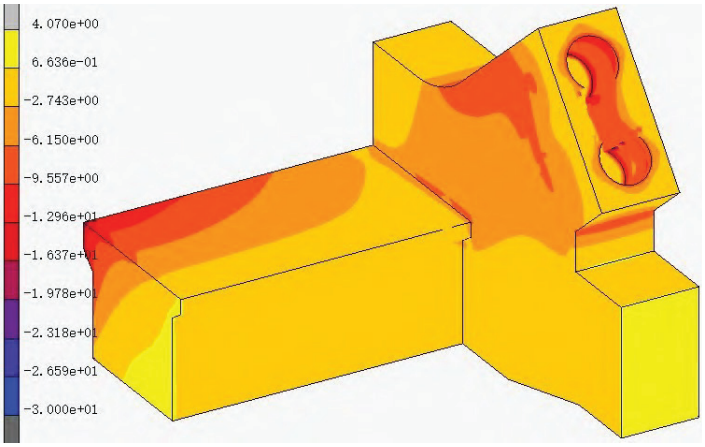

Figure 7 Cloud diagram of the maximum principal compressive stress in the arch seat concrete.

stress appears at the intersection of arch rib, arch foot, and tie beam, which is because the force there is more complex, with the support reaction force of the support, the axial force transmitted by the cross beam, the bending moment and axial force transmitted by the arch rib and the transfer effect of the longitudinal beam to it. 1.51 MPa, less than the concrete tensile stress 2.65 MPa, to meet the requirements. When designing here, the designer should optimize the stresses at the location where the crossbeam, longitudinal beam, and arch rib are connected.

Secondly, in the stress analysis of steel tube concrete, as can be seen from Figure 7, the main compressive stress of steel tube concrete is generally evenly distributed from the inside to the outside. This is because the Poisson's ratio of concrete is greater than that of steel, and under axial compression, the deformation of concrete is greater than that of the steel tube, so the steel tube forms a hoop effect on the concrete, and the maximum principal compressive stress occurs at the connection between the arch rib and the abutment. The maximum compressive stress at the connection between the arch rib and the abutment is 25.22 MPa, while the compressive stress of the other concrete is less than 31.9 MPa, which is less than the compressive strength of C50 concrete, and satisfies the load-bearing requirements. The main tensile stress of concrete inside the steel tube is less than 2.71 MPa, except for a small amount of stress concentration at the intersection of the end crossbeam, arch foot and tie beam, which meets the load-bearing requirements.

Modeling is carried out according to the design drawings. The finite element model includes: a dumbbell-shaped arch rib with a length of 2.0 m protruding from the arch foot, the solid part of the arch foot, and an end beam with a half length of 5.95 m. Through the calculation of the bar system model of the whole bridge, the most unfavorable load of the arch foot is combined to the internal force of the arch rib section, and the cross-sections of the arch rib and longitudinal beam are respectively loaded, the supporting reaction force is applied at the bottom of the arch foot, and the end beam is consolidated. Among them, a support reaction force of 23790 kN is applied at the arch foot %, an s force of 30253 kN, a shear force of 56 kN, and a bending moment of 3839 kN·m are applied at the arch i, and an s force of 18936 kN and a shear force of 135 kN are applied at the truncated interface of the longitudinal beam. Bending moment of 2033 kN·m.

5.3 Analysis of Results

Figure 8 shows the relationship between the displacement of each measurement point and the load variation for loading conditions 1 and 2. It can be seen from Figure 8 that the structure exhibits good elastic response when the load is less than 2000 kN. However, when the load reaches 2400 kN, the deformation of the component decreases significantly with the load variation, which is related to the load-sharing ratio between the inner steel tube and outer steel sleeve. At the same time, it can be seen from Figure 8 that compared with the first loading of condition 2, the deformation of the specimen has decreased significantly, but it still shows good elasticity, indicating that the specimen has entered the yield stage. The load-sharing ratio between the inner steel

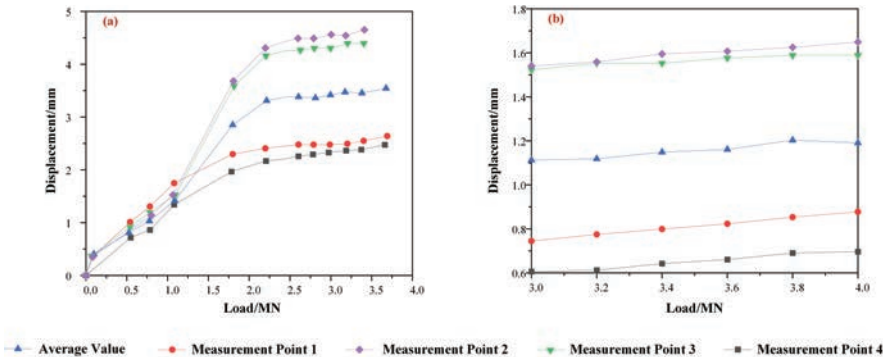

Figure 8 Load-displacement curve of each measurement point during loading.

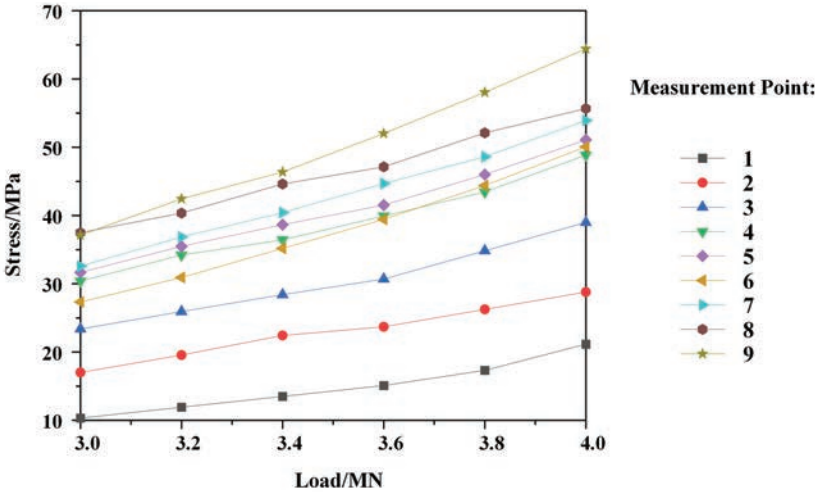

Figure 9 Load-stress curves of the measured points of the outer steel sleeve wall.

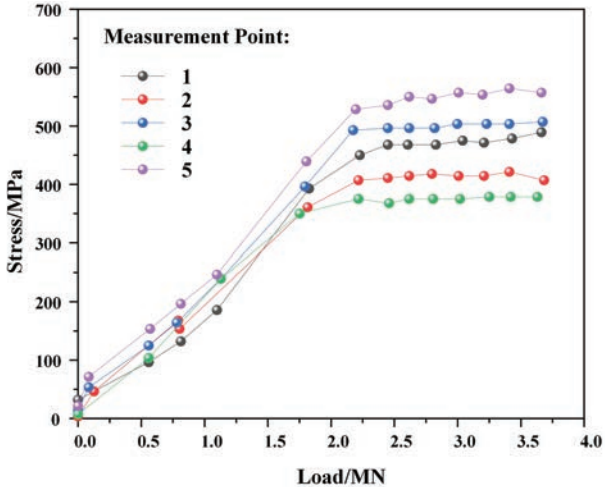

Figure 10 Steel pipe loading point compressive stress value within the working condition 1.

tube and outer steel sleeve changes during this stage, but the overall bearing capacity of the structure is still greater than 4000 kN.

Figure 9 shows the load-stress change curve of each measurement point of the outer steel sleeve when loaded in load case 2. From Figure 9, it can be seen that the outer steel sleeve always maintains a low-stress state, and the stress at the top of the outer steel sleeve is slightly less than the stress at the middle

measurement points. Figure 10 is the inner steel tube load-stress relationship change curve, from Figure 10 can be seen, in the 1800 kN load, the inner steel tube began to enter the yielding stage, with the increase in load, most of the measurement point stress does not increase, but the residual stress is larger. During the test process of the inner steel tube into the plastic working state, but not destroyed, the entire test process, the inner steel tube always bear greater stress than the outer steel sleeve, which has some differences from the actual structure of the inner steel tube stress, mainly with the model specimen production, the inner steel tube, the outer steel sleeve and the bottom bearing surface contact.

6 Conclusion

This paper takes a steel pipe concrete arch bridge as an example, carries out the proposed static test and finite element simulation test of the SFRP material specimen, intercepts the geometry of its arch rib foot position for finite element analysis, the overall structural deformation, the arch foot SFRP stress situation, the steel pipe in the concrete stress situation to analyze the following conclusions:

(1) The maximum area of the hysteresis loop usually appears near the peak stress of the material, and as the surrounding pressure increases, the stress point corresponding to the largest area of the hysteresis loop is then delayed. With the increasing value of the enclosing pressure, the peak stress corresponds to the peak strain after which the strain increases significantly, but the stress does not change much. The material stress-strain curve tends to flatten out, reflecting the characteristics of plastic deformation, and the peak stress of the material increases significantly.

(2) Except for very few points, the maximum principal compressive stress is 30 MPa, which meets the requirements; the maximum principal tensile stress appears at the intersection of the arch rib, arch foot, and tie beam, which is 1.51 MPa, less than the concrete tensile stress of 2.65 MPa, which meets the requirements. The maximum compressive stress is 24.31 MPa at the connection of the arch rib and arch seat; except for a small amount of stress concentration at the junction of the end crossbeam, arch foot, and tie beam, the main tensile stress is greater than the concrete tensile stress of 2.65 MPa, which meets the requirements. The maximum equivalent stress appears in the middle of the end pipe of the arch rib, which is 110.5 MPa, less than the yield stress of 345 MPa, which meets the requirements.

(3) The designer should focus on the stress at the connection position of the crossbeam, longitudinal beam, and arch rib and the wall thickness of the steel pipe when carrying out the design. This paper can provide a reference for related projects.
(4) The stress-strain curve of the steel fiber reinforced concrete material under the action of triaxial cyclic loading and unloading appears a closed loop area, that is, the hysteresis loop effect. The largest area of the hysteresis loop usually appears near the peak stress of the material, and as the confining pressure increases, the stress point corresponding to the largest hysteresis loop appears later. With the continuous increase of the confining pressure, the strain increases significantly after the peak strain corresponding to the peak stress, but the stress changes little. The stress-strain curve of the material tends to be flat, reflecting the characteristics of plastic deformation, and the peak stress of the material increases obviously.

References

[1] Centonze, G., M. Leone, and M. A. Aiello. "Steel fibers from waste tires as reinforcement in concrete: A mechanical characterization." Construction and Building Materials 36 (2012): 46–57.
[2] Dib, Antoine. "The Development of a New Hysteretic Device: The Crescent Shaped Brace." (2017).
[3] Marcos-Meson, V., et al. "Durability of Steel Fibre Reinforced Concrete (SFRC) exposed to acid attack–A literature review." Construction and Building Materials 200 (2019): 490–501.
[4] Bolander, John E., et al. "Discrete mechanical models of concrete fracture." Engineering Fracture Mechanics 257 (2021): 108030.
[5] Hasan, Mahadi, Jingwei Zhao, and Zhengyi Jiang. "Micromanufacturing of composite materials: a review." International Journal of Extreme Manufacturing 1.1 (2019): 012004.
[6] Gong, Chenjie, et al. "Comparison of the structural behavior of reinforced concrete and steel fiber reinforced concrete tunnel segmental joints." Tunnelling and Underground Space Technology 68 (2017): 38–57.
[7] Tiberti, Giuseppe, Fausto Minelli, and Giovanni Plizzari. "Reinforcement optimization of fiber reinforced concrete linings for conventional tunnels." Composites Part B: Engineering 58 (2014): 199–207.

[8] Liu, Xian, et al. "Comparison of the structural behavior of reinforced concrete tunnel segments with steel fiber and synthetic fiber addition." Tunnelling and Underground Space Technology 103 (2020): 103506.

[9] Ruiz, Gonzalo, Angel de la Rosa, and Elisa Poveda. "Relationship between residual flexural strength and compression strength in steel-fiber reinforced concrete within the new Eurocode 2 regulatory framework." Theoretical and Applied Fracture Mechanics 103 (2019): 102310.

[10] Yang, Kai, Qixiang Yan, and Chuan Zhang. "Three-dimensional mesoscale numerical study on the mechanical behaviors of SFRC tunnel lining segments." Tunnelling and Underground Space Technology 113 (2021): 103982.

[11] Abbas, Safeer, and Moncef L. Nehdi. "Mechanical Behavior of Ultrahigh-Performance Concrete Tunnel Lining Segments." Materials 14.9 (2021): 2378.

[12] Raju, Ramiz Ahmed, et al. "Effects of concrete flow on the distribution and orientation of fibers and flexural behavior of steel fiber-reinforced self-compacting concrete beams." Construction and Building Materials 262 (2020): 119963.

[13] Huang, Guoqing, Na Ren, and Hengbin Zheng. "Structural Dynamics of Bridges Under the Coupling Effect of Windmills and Bridges." European Journal of Computational Mechanics (2022): 601–620.

[14] Caggiano, Antonio, et al. "Fracture behavior of concrete beams reinforced with mixed long/short steel fibers." Construction and Building Materials 37 (2012): 832–840.

[15] Hsu, Tai-Ran. "Miniaturization–A paradigm shift in advanced manufacturing and education." International conference on Advanced Manufacturing Technologies and Education in the 21st Century. 2002.

[16] Murali, Gunasekaran, et al. "Combined effect of multi-walled carbon nanotubes, steel fibre and glass fibre mesh on novel two-stage expanded clay aggregate concrete against impact loading." Crystals 11.7 (2021): 720.

[17] Romualdi, James P., and Gordon B. Batson. "Mechanics of crack arrest in concrete." Journal of the Engineering Mechanics Division 89.3 (1963): 147–168.

[18] Bos, Freek, et al. "Additive manufacturing of concrete in construction: potentials and challenges of 3D concrete printing." Virtual and physical prototyping 11.3 (2016): 209–225.

[19] Gonçalves, R. M., A. Martinho, and J. P. Oliveira. "Evaluating the potential use of recycled glass fibers for the development of gypsum-based composites." Construction and Building Materials 321 (2022): 126320.
[20] Fang, Yunsheng, et al. "Smart textiles for personalized thermoregulation." Chemical Society Reviews 50.17 (2021): 9357–9374.
[21] Ramkumar, K. B., and Kannan Rajkumar PR. "Impact of hybrid steel fibres on fresh and mechanical properties of Self-compacting concrete." Case Studies in Construction Materials 17 (2022): e01274.
[22] Cogswell, Frederic Neil. Thermoplastic aromatic polymer composites: a study of the structure, processing and properties of carbon fibre reinforced polyetheretherketone and related materials. Elsevier, 2013.
[23] Wang, Xing Quan, Cheuk Lun Chow, and Denvid Lau. "A review on modeling techniques of cementitious materials under different length scales: Development and future prospects." Advanced Theory and Simulations 2.7 (2019): 1900047.
[24] Chen, Le, et al. "Multiscale study of fibre orientation effect on pullout and tensile behavior of steel fibre reinforced concrete." Construction and Building Materials 283 (2021): 122506.
[25] Zhao, Chenggong, et al. "Research on different types of fiber reinforced concrete in recent years: An overview." Construction and Building Materials 365 (2023): 130075.
[26] Huang, Qian, et al. "innovative design of novel main and secondary arch collaborative Y-shaped arch bridge and research on shear lag effect of its unconventional thin-walled steel box arch ribs." Applied Sciences 12.16 (2022): 8370.
[27] Rezaiee-Pajand, Mohammad, and Arash Karimipour. "Stress analysis by two cuboid isoparametric elements." European Journal of Computational Mechanics (2019): 373–410.
[28] Bouziane, Salah, Hamoudi Bouzerd, and Mohamed Guenfoud. "Mixed finite element for modelling interfaces." European Journal of Computational Mechanics 18.2 (2009): 155–175.

Biographies

Liu Kailiang received his bachelor's degree in engineering from Zhongyuan University of Technology in 2006, followed by a master's degree in Materials from Université Claude Bernard Lyon 1 in Lyon, France. Currently, he serves as a professor at the Department of Railway Engineering at Zhengzhou Railway Vocational & Technical College, focusing his research on Construction Materials and Green Construction Materials.

Wang Sen was born in Henan, China in 1996. From 2014 to 2018, he studied at Huanghuai University and obtained a bachelor's degree in 2018, and from 2018 to 2020, he studied at Henan University and obtained a master's degree in 2020. Since 2020, he has been working at Zhengzhou Railway Vocational and Technical College. He has published three papers, one of which has been included in the Peking University Core. His research interests include Engineering Management and Smart City.